

Validation of Lasing in Active Nanocavities

Yong-Seok Choi,^{1,*} Matthew T. Rakher,² Kevin Hennessy,¹ Stefan Strauf,^{2,3}
Antonio Badolato,¹ Pierre M. Petroff,^{1,3} Dirk Bouwmeester,² and Evelyn L. Hu^{1,3}

¹*ECE Department, University of California Santa Barbara, CA 93106, Santa Barbara, USA*

²*Department of Physics, University of California Santa Barbara, CA 93106, Santa Barbara, USA*

³*Materials Department, University of California Santa Barbara, CA 93106, Santa Barbara, USA*

(Dated: May 24, 2019)

An unambiguous proof of lasing in an active nanocavity with ultrahigh spontaneous emission coupling factor ($\beta = 0.65$) is presented. To distinguish the subtle lasing threshold features from possible material-related phenomena, such as saturable absorption in the gain medium, a series of active nanocavities with different values of β have been designed to systematically approach the high- β device. The demonstration of the lasing threshold is obtained through the observation of the transition from thermal to coherent light photon statistics that is well understood and identified in the $\beta \ll 1$ lasing regime. The systematic investigation allows a more definitive validation of the onset of lasing in these active nanocavities.

PACS numbers: 42.55.Tv, 78.67.Hc, 78.55.Cr, 42.50 Ar

Advances in fabrication of optical nano-scale devices enable the construction of nanolasers in which there is effectively only one optical emission mode. The β factor is a measure inversely proportional to the number of available modes in which the gain medium can spontaneously emit photons. Achieving a high β factor is a key issue for improving single-photon sources [1, 2, 3]. In addition, high β values enable low-threshold lasers with high modulation speeds [4] and low intensity noise [5]. Various semiconductor laser systems have demonstrated high β values of order of 0.1 [6, 7, 8, 9], and in particular, recent achievements in quantum dot nanocavities have demonstrated close-to-perfect coupling efficiencies [10, 11, 12, 13]. For such devices with β approaching unity, the lasing threshold is harder to determine and shifts to very low optical pump and output powers (the hypothetical case of a $\beta = 1$ is often referred to as a thresholdless laser [4]). The characteristic nonlinearities in the optical output power and the emission linewidth around the lasing threshold become so subtle that one might wonder whether other effects such as saturable absorption in the optical gain medium could be responsible for the observed features [14]. The question of what constitutes a laser becomes even more intricate if an unconventional gain medium, e.g. consisting of a very low density of optically active quantum dots, is considered.

In this Letter, we provide validation of the existence of a lasing threshold in a β factor of nearly unity laser that is independent of the precise gain mechanism and the (nonlinear) absorption characteristics of the material. The validation is based on the design and fabrication of a series of nanocavities that support dominantly, one, two and three optical modes overlapping with the gain medium. This stepwise decreases the β factor from approximately 1 to 0.5 to 0.33 (in our experiments from 0.65 to 0.35 to 0.15) and brings the observed transition features into the regime where they are unambiguously

identified as the lasing threshold. As the defining signature of the lasing threshold, we use the transition from the thermal light source to the coherent light source as measured by the second-order intensity correlation function:

$$g^{(2)}(\tau) = \frac{\langle E^{(-)}(t)E^{(-)}(t+\tau)E^{(+)}(t+\tau)E^{(+)}(t) \rangle}{\langle \langle E^{(-)}(t)E^{(+)}(t) \rangle \rangle^2} \quad (1)$$

where $E^{(+)}(t)$ and $E^{(-)}(t)$ are the positive and negative frequency parts of the electromagnetic field, respectively [15]. The measurement of $g^{(2)}(\tau)$ reveals a fundamental difference between a laser, i.e. $g^{(2)}(\tau) = 1$, and thermal light, i.e. $g^{(2)}(0) = 2$ [16]. The interpretation of the observed-laser-photon statistics [17, 18] led to the quantum theory on coherent-state transitions [19, 20].

We consider nanocavities with a gain medium comprised of a low density ($\sim 5 \times 10^9/\text{cm}^2$) of InAs quantum dots (QDs) grown by a partially covered island technique [21]. Nanocavities were designed to support one, two, and three modes in the s-shell region of QDs, and hence to reveal the effect of β on laser photon statistics systematically. Nanocavities utilize the triangular-lattice photonic-crystal (PC) structures with three, seven, and eleven missing holes in the Γ - K direction, denoted as L3, L7, and L11 cavities, respectively. The conditions for cavity resonances are determined by the PC waveguide dispersion and the Fabry-Perot condition [22]. FIG. 1(a) shows the dispersion curves of a single-line-defect PC waveguide and the resonant modes of L7 and L11 cavities calculated by the three-dimensional (3D) finite-difference time-domain (FDTD) method. To use the low energy, high- Q even (e#) modes below the light line, we specified a lattice constant of ~ 260 nm, a hole radius of ~ 65 nm, and a membrane thickness of ~ 126 nm in the processing [11]. An L7 cavity is shown in the scanning electron micrograph (SEM) inset of FIG. 1(a).

The experimental setup consists of a He-cryostat,

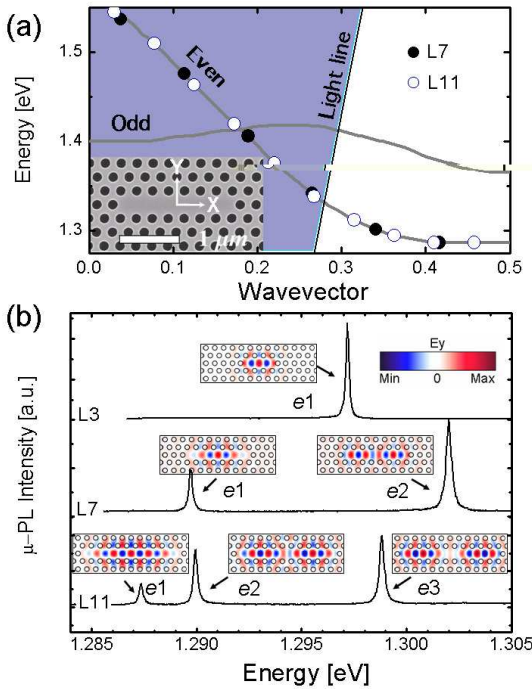


FIG. 1: (a) The dispersion curves of a single-line-defect PC waveguide and the resonances of the L7 and L11 cavities obtained by 3D FDTD, where the shaded region is a leaky region. An inset shows the SEM of an L7 cavity. (b) Calculated E_y field profiles identify resonant peaks in the μ -PL spectra.

micro-photoluminescence (μ -PL) system, and a photon correlation measurement apparatus with two avalanche photodiodes (APDs) in the Hanbury-Brown Twiss configuration. The QD PC nanolasers were optically pumped by a power and temperature stabilized 780 nm diode laser. FIG. 1(b) shows the μ -PL spectra of L3, L7, and L11 cavities with one, two, and three modes, respectively. All the modes are polarized in the Y direction with no degeneracy. Provided that these nanocavity modes are decorated by the broad QD gain spectrum [13], the maximum β is 1 for L3, 0.5 for L7, and 0.33 for L11 cavities.

To explore the lasing behavior of the QD PC nanocavities, we can inspect a typical output characteristics of an L3 laser, plotted as a function of the incident pump power as shown in FIG. 2(a). The output starts to grow nonlinearly, and then increases in a nearly linear manner before being clamped at values of incident pump powers above 20 μ W. The dependence of $g^{(2)}(0)$ on the incident pump power is compared with the output characteristics in FIG. 2(a). $g^{(2)}(0)$ increases with incident power from 0.2 μ W to 0.6 μ W, subsequently converging to one before the output emission is clamped. FIG. 2(b) is the $g^{(2)}(\tau)$ plot taken at 0.6 μ W, which shows the largest bunching peak for the L3 laser. This maximum bunching plot for the L3 structure can be compared with the

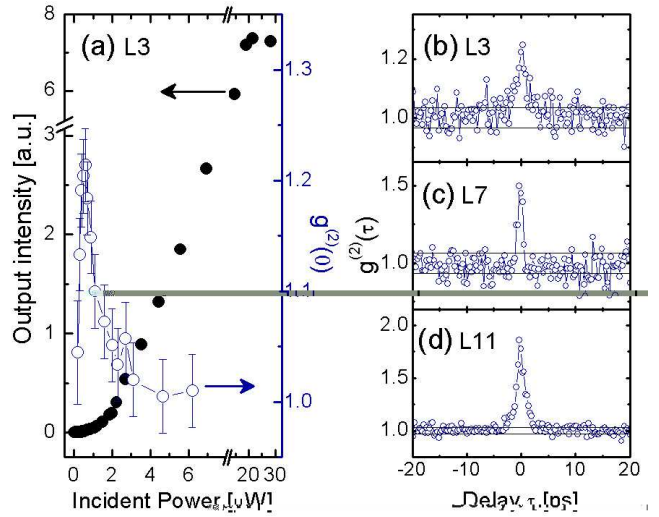


FIG. 2: (a) The output intensity and the $g^{(2)}(0)$ graph of an L3 laser as a function of the incident power. The $g^{(2)}(\tau)$ spectra with maximum bunching behaviors observed in (b) L3, (c) L7, and (d) L11 lasers, respectively. In the $g^{(2)}(\tau)$ measurements, the spectral window was set by the 0.5 nm bandpass filters attached to the APDs. The APD detection rates were kept to be 10^4 - 10^5 at various pump powers. A coincidence value at long delay time ($\tau > 100$ ns) was taken as a reference for normalization. Parallel lines in (b)-(d) indicate the standard deviation noise.

similar plots for the L7 and L11 lasers, shown in FIGS. 2(c) and 2(d). Note that there are systematic variations in the peak value of $g^{(2)}(\tau)$, the width of the bunching peak, and the signal to noise of the curves. These variations are the natural outcome of the different values of β , determined by the number of allowed cavity modes in the different structures, as we will show below. One immediate question raised by the data of FIG. 2(a) is the decrease of $g^{(2)}(0)$ below threshold, as it should be super-Poissonian with $g^{(2)}(0) = 2$ [16].

To gain further understanding into this discrepancy, we sought insight through calibration measurements of a more conventional GaAlAs MQW laser that also serves as the pump source for our QD PC nanolasers. The laser displays a clear threshold current of 36.25 mA as shown in FIG. 3(a). Below threshold, the MQW gain spectrum decorates about 100 cavity modes with a mode spacing of 0.13 nm. To discriminate side modes in the photon correlation measurements, we replaced the 0.5 nm bandpass filters by a monochromator with a bandwidth as narrow as the lasing mode linewidth. Pronounced bunching signals in $g^{(2)}(\tau)$ were observed in the narrow current region from $0.88 \times I_{th}$ to $1.01 \times I_{th}$. The bunching height, i.e. $g^{(2)}(0)$, increases as the current is elevated to $0.986 \times I_{th}$ and rapidly converges to one as shown in FIG. 3(b). The bunching width, i.e. $\Delta\tau$, is nearly constant (~ 1 ns) with operating currents from $0.88 \times I_{th}$ to $0.97 \times I_{th}$ where $g^{(2)}(0)$ changes from 1.1 to 1.5. Then, $\Delta\tau$ grows with

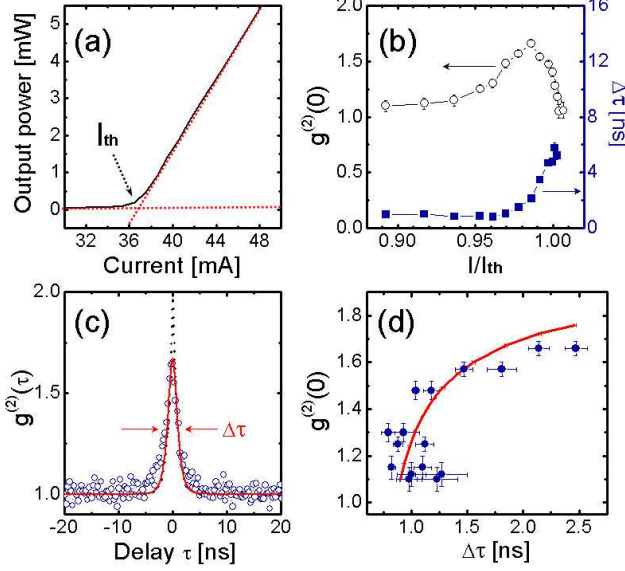


FIG. 3: (a) The output power of the MQW laser as a function of current I . (b) $g^{(2)}(0)$ and $\Delta\tau$ as a function of I/I_{th} . (c) The experimental (open circles) and theoretical $g^{(2)}(\tau)$ spectra, where the dashed line is the ideal $g^{(2)}(\tau)$ while the solid line is the simulated $g^{(2)}(\tau)$ with $M(t, \sigma = 450\text{ps})$. (d) The effect of $M(t, \sigma)$ on $g^{(2)}(0)$ and $\Delta\tau$, where dots are the experimental data and the line is a simulation.

the increase of operating current as shown in FIG. 3(b). The observed behaviors of $g^{(2)}(0)$ and $\Delta\tau$ over threshold are expected as the emission becomes more coherent. But, the absolute value of $g^{(2)}(0)$ below threshold is naively expected to obtain the value of 2 that does not match the data. This can be explained by taking into account the limited temporal resolution of 450 ps of our setup. When the coherence time of the light source becomes comparable to the temporal resolution of the measurement system, then the $g^{(2)}(\tau)$ below threshold, which is normally given by $g^{(2)}(\tau) = 1 + \exp[-2|\tau|/\tau_c]$, must be convolved with a measurement function $M(t, \sigma) = (\sigma\sqrt{2\pi})^{-1}\exp[-t^2/2\sigma^2]$, where σ is the APD timing jitter. FIG. 3(c) shows the ideal and simulated $g^{(2)}(\tau)$ functions for $\tau_c = 2$ ns and $\sigma = 450$ ps. The simulation shows that $g^{(2)}(0)$ is reduced by 0.3, in good agreement with the experimental data taken at $0.986 \times I_{th}$. We examined the effect of $M(t, \sigma)$ for various values of τ_c from 0.1 ns to 2 ns, and the results are plotted with the experimental data in FIG. 3(d), showing excellent agreement. The calibration measurements underscore the importance of adequate timing resolution for sources with short coherence times. These measurements also demonstrate that the genuine signature of lasing action is the convergence of $g^{(2)}(0)$ to one above threshold.

To complete our quantitative analysis of the variation of $g^{(2)}(0)$ with pump power, the identification of the onset of lasing, and the correlations among QD PC nanolasers

with different β values, we first calculate the photon number probability (p_n), given by [20, 23],

$$p_n = p_0 \prod_{k=1}^{k=n} \frac{N_a}{N_b + 2T_1(R^{-1} + k)\kappa}, \quad (2)$$

where p_0 is the zero photon probability and can be determined by normalization, n is the number of photons in the cavity, and N_a and N_b are the number of carriers in the upper and the lower levels, respectively. T_1 is defined by $T_1 = (\Lambda_0 + \gamma')^{-1}$, where Λ_0 is the pumping rate and γ' is the sum of all recombination rates that do not add a photon to the cavity mode. R is defined by $R = 4g^2 T_1 T_2$, where g is the coupling parameter between the cavity mode and the excitonic transitions of carriers, and T_2 is the dephasing time. κ is the cavity decay rate given by $\kappa = 2\pi\nu/Q$, where ν is the frequency of the cavity mode. The normalized zero-field populations of the upper and lower laser levels are given by $N_a = N\Lambda_0 T_1$ and $N_b = N\gamma' T_1$, where N is the total number of carriers that correspond to gain saturation.

To investigate the effect of β on the laser photon statistics, we adopted the phenomenological expression [24],

$$\beta = \left[1 + \frac{\gamma'}{2g^2} \left(\frac{1}{T_2} + \frac{\kappa}{2} \right) \right]^{-1}, \quad (3)$$

which is simply the ratio of the spontaneous emission rate into the cavity mode to the total recombination rate. We used β and N as fitting parameters to best describe the observed $g^{(2)}(0) \rightarrow 1$ behavior with the increase of the pump power. Here, N rather than the number of QDs was introduced as a fitting parameter to account for the non-resonant optical pumping scheme. In contrast to the resonant optical excitation of QD energy levels, photo-generated carriers in the GaAs bulk region relax to the wetting layer (WL) and to QDs. In this process, the efficient coupling between the rich WL density of states and QDs is believed to be fast enough to repopulate QDs contributing to lasing action [13]. For the QD PC nanolasers at 4 K, γ' can be obtained by $2\pi/\tau_{PL}$ according to the μ -PL decay time ($\tau_{PL} \sim 5$ ns) measured for a QD uncoupled to the cavity mode. The theoretical analysis was unaffected by taking T_2 in the range of 0.1 ns to 1 ns [2, 25]. For the GaAlAs MQW laser at the room temperature, we can use the typical parameters of γ' of 1.0 GHz and T_2 of 0.1 ps and N of 5×10^7 [23]. Other parameters used in calculation are summarized in Table I.

Based on this analysis, the theoretical $g^{(2)}(0)$ curves were obtained as shown in FIG. 4. The change of $g^{(2)}(0)$ at the vicinity of I_{th} in the MQW laser agrees with the theoretical curve indicated by a solid line, which was obtained with β of 0.0001 and typical parameters shown in Table I. Furthermore, the theoretical curve below threshold shows the expected behavior of $g^{(2)}(0) = 2$. If we simulate the experimental values of $g^{(2)}(0)$ with

TABLE I: We summarize the spontaneous emission coupling factor β , the cavity decay rate κ , the exciton-cavity coupling parameter g , and the number of carriers N for QD PC nanolasers and the conventional MQW laser.

Device	β	κ [GHz]	g [GHz]	N
L3	0.65 ± 0.05	287	13 ± 2	$(3.2 \pm 0.7) \times 10^2$
L7	0.35 ± 0.05	432	8.6 ± 1.0	$(1.1 \pm 0.2) \times 10^3$
L11	0.15 ± 0.025	396	4.7 ± 0.5	$(3.3 \pm 0.5) \times 10^3$
MQW laser	0.0001	200	0.7	5×10^7 [23]

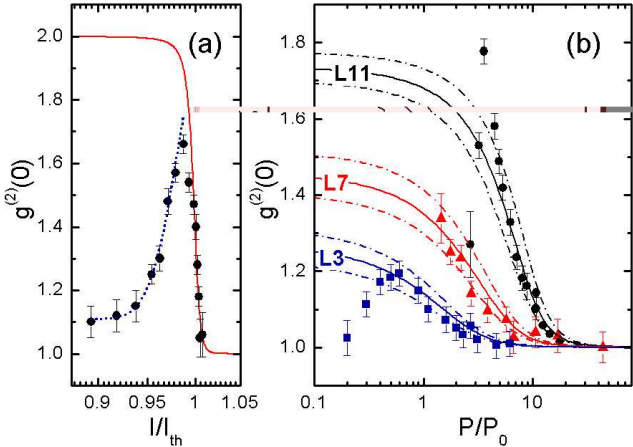


FIG. 4: (a) The experimental $g^{(2)}(0)$ data (dot) of the MQW laser with the theoretical curve (solid line) obtained by $\beta = 0.0001$. The dotted line shows the effect of a temporal resolution on the measurement of $g^{(2)}(0)$, when the ideal $g^{(2)}(0)$ is given by the solid line. (b) The experimental $g^{(2)}(0)$ data of L3, L7, L11 lasers with the theoretical curves obtained by the β of 0.65 ± 0.05 , 0.35 ± 0.05 , and 0.15 ± 0.025 , respectively. The dash-dot lines indicate the upper and lower bounds of fits considering the given uncertainties of β factors.

this theoretical curve and $M(t, \sigma=450\text{ps})$, we can obtain the dotted line, which is in good agreement with the experimental data. The theoretical curves for QD PC nanolasers are summarized in FIG. 4(b). The systematic variation of the $g^{(2)}(0)$ values can be seen with the expected β values of 0.65 ± 0.05 , 0.35 ± 0.05 , and 0.15 ± 0.025 for the L3, L7, and L11 cavities, respectively. Here, the fits have been made to best describe the transition of $g^{(2)}(0)$ with the increase of the pump power, even if the initial bunching behaviors are yet to be clarified with better temporal resolution and detection efficiency. But, both the experimental and theoretical results demonstrate slow coherent-state transitions [26], distinguishing high- β QD PC nanolasers from the conventional MQW laser. The theoretical $g^{(2)}(0)$ curves below threshold show saturation behaviors that decrease as β increases, which is expected as β approaches unity and coherence is observed for all input pump powers. This can be explained by the fact that high- β devices have a significant contribution from spontaneous emission into

the lasing mode even at very low pump powers, which destroys a thermal field description with $g^{(2)}(0) = 2$.

In conclusion, we have demonstrated the systematic correlation between the coherent-state transition and the lasing action in QD PC nanocavities. The onsets of coherence in soft-turn-on nanolasers are confirmed by the convergence to Poissonian statistics, i.e. $g^{(2)}(0) = 1$, with the increase of the pump power. The bunching behavior near threshold is found to subside with the increase of β . The quantitative analysis reveals the very high β of 0.65 , 0.35 , and 0.15 , as predicted for the L3, L7, and L11 cavities, respectively. This general approach of constructing a series of nano devices with the limiting case as the device of interest, might prove useful to identify other features in nano devices that can be difficult to distinguish from material properties.

This work was funded under DARPA No. 972-01-1-0027, DMEA No. H94003-04-2-0403, and NSF NIRT No. 0304678.

* Corresponding author: cys@cnsi.ucsb.edu

- [1] P. Michler *et al.*, *Science* **290**, 2282 (2000).
- [2] C. Santori *et al.*, *Nature* **419**, 594 (2002).
- [3] Z. Yuan *et al.*, *Science* **295**, 102 (2002).
- [4] H. Yokoyama and S. D. Brorson, *J. Appl. Phys.* **66**, 4801 (1989); H. Yokoyama, *Science* **256**, 66 (1992).
- [5] G. Björk, A. Karlsson, and Y. Yamamoto, *Phys. Rev. A* **50**, 1675 (1994).
- [6] R. E. Slusher *et al.*, *Appl. Phys. Lett.* **63**, 1310 (1993).
- [7] T. Baba, *IEEE. J. Sel. Topics Quant. Elec.* **3**, 808 (1997).
- [8] O. Painter *et al.*, *Science* **284**, 1819 (1999).
- [9] H.-G. Park *et al.*, *Science* **305**, 1444 (2004).
- [10] M. Pelton *et al.*, *Phys. Rev. Lett.* **89**, 233602 (2002).
- [11] A. Badolato *et al.*, *Science* **308**, 1158 (2005); K. Hennessee *et al.*, *Photonics Nanostruct. Fundam. Appl.* **2**, 65 (2004).
- [12] A. Kress *et al.*, *Phys. Rev. B* **71**, 241304 (2005).
- [13] S. Strauf *et al.*, submitted to *Phys. Rev. Lett.* Available at arxiv/cond-mat/0511494.
- [14] N. G. Stoltz *et al.*, *Appl. Phys. Lett.* **87**, 031105 (2005).
- [15] R. J. Glauber, *Phys. Rev.* **130**, 2529 (1963).
- [16] F. T. Arecchi, E. Gatti, and A. Sona, *Phys. Lett.* **20**, 27 (1966).
- [17] C. Freed and H. A. Haus, *Phys. Rev. Lett.* **15**, 943 (1965).
- [18] A. W. Smith and J. A. Armstrong, *Phys. Rev. Lett.* **16**, 1169 (1966).
- [19] M. O. Scully and W. E. Lamb, Jr. *Phys. Rev.* **179** 368 (1969); V. DeGiorgio and M. O. Scully, *Phys. Rev. A* **2**, 1170 (1970).
- [20] P. Filipowicz, J. Javanainen, and P. Meystre, *Phys. Rev. A* **34**, 3077 (1986).
- [21] J. M. García *et al.*, *Appl. Phys. Lett.* **72**, 3172 (1998).
- [22] S.-H. Kim *et al.*, *J. Appl. Phys.* **95**, 411 (2004).
- [23] R. Jin *et al.*, *Phys. Rev. A* **49**, 4038 (1994).
- [24] I. Protsenko *et al.*, *Phys. Rev. A* **59**, 1667 (1999).
- [25] P. Borri *et al.*, *Phys. Rev. Lett.* **87**, 157401 (2001).
- [26] P. R. Rice and H. J. Carmichael, *Phys. Rev. A* **50**, 4318 (1994).